J|A|C|S
ARTICLES
Published on Web 06/07/2006

Carbonic Anhydrase Inhibitors: X-ray and Molecular Modeling Study for the Interaction of a Fluorescent Antitumor Sulfonamide with Isozyme II and IX

Vincenzo Alterio,[†] Rosa Maria Vitale,[†] Simona Maria Monti,[†] Carlo Pedone,[†,‡] Andrea Scozzafava,[§] Alessandro Cecchi,[§] Giuseppina De Simone,*[,†] and Claudiu T. Supuran*[,§]

Contribution from the Istituto di Biostrutture e Bioimmagini-CNR, via Mezzocannone 16, 80134 Naples, Italy, Dipartimento delle Scienze Biologiche-Sezione Biostrutture, University of Naples "Federico II", via Mezzocannone 16, 80134 Naples, Italy, and Università degli Studi di Firenze, Polo Scientifico, Laboratorio di Chimica Bioinorganica, Rm. 188, Via della Lastruccia 3, 50019 Sesto Fiorentino (Florence), Italy

Received March 7, 2006; E-mail: gdesimon@unina.it; claudiu.supuran@unifi.it

Abstract: The X-ray crystal structure of the fluorescent antitumor sulfonamide carbonic anhydrase (CA, EC, 4.2.1.1) inhibitor (4-sulfamoylphenylethyl)thioureido fluorescein (**1**) in complex with the cytosolic isoform hCA II is reported, together with a modeling study of the adduct of **1** with the tumor-associated isoform hCA IX. Its binding to hCA II is similar to that of other benzesulfonamides, with the ionized sulfonamide coordinated to the Zn^{2+} ion within the enzyme active site, and also participating in a network of hydrogen bonds with residues Thr199 and Glu106. The scaffold of **1** did not establish polar interactions within the enzyme active site but made hydrophobic contacts (<4.5 Å) with Gln92, Val121, Phe131, Val135, Leu198, Thr199, Thr200, and Pro202. The substituted 3-carboxy-amino-phenyl functionality was at van der Waals distance from Phe131, Gly132, and Val135. The bulky tricyclic fluorescein moiety was located at the rim of the active site, on the protein surface, and strongly interacted with the α-helix formed by residues Asp130-Val135. All these interactions were preserved in the hCA IX−**1** adduct, but the carbonyl moiety of the fluorescein tail of **1** participates in a strong hydrogen bond with the guanidine moiety of Arg130, an amino acid characteristic of the hCA IX active site. This may account for the roughly 2 times higher affinity of **1** for hCA IX over hCA II and may explain why in vivo the compound specifically accumulates only in hypoxic tumors overexpressing CA IX and not in the normal tissues. The compound is in clinical studies as an imaging tool for acute hypoxic tumors.

Introduction

At least 16 isoforms of the widely spread metalloenzyme carbonic anhydrase (CA, EC 4.2.1.1) were discovered up to now in humans, all belonging to the α-CA gene family.[1−5] These are hCA I−hCA XV, but there are two mitochondrial enzymes denominated hCA VA and hCA VB,[6,7] which leads to the final number of 16 isoforms. Many of them constitute interesting targets for the design of pharmacological agents useful in the treatment or prevention of a variety of disorders such as glaucoma,[3,8−10] acid−base disequilibria,[11] epilepsy[12,13] and other neuromuscular diseases,[14] altitude sickness,[15] edema,[16] and obesity.[17,18] A quite new and unexpected application of the CA inhibitors (CAIs) regards their potential use in the management (imaging and treatment) of hypoxic tumors,[19] since some CAs

[†] Istituto di Biostrutture e Bioimmagini-CNR.
[‡] University of Naples "Federico II".
[§] Università degli Studi di Firenze.

(1) Pastorekova, S.; Parkkila, S.; Pastorek, J.; Supuran, C. T. *J. Enzyme Inhib. Med. Chem.* **2004**, *19*, 199−229.
(2) Lehtonen, J.; Shen, B.; Vihinen, M.; Casini, A.; Scozzafava, A.; Supuran, C. T.; Parkkila, A. K.; Saarnio, J.; Kivela, A. J.; Waheed, A.; Sly, W. S.; Parkkila, S. *J. Biol. Chem.* **2004**, *279*, 2719−2727.
(3) Supuran, C. T.; Scozzafava, A.; Casini, A. *Med. Res. Rev.* **2003**, *23*, 146−189.
(4) Supuran, C. T.; Vullo, D.; Manole, G.; Casini, A.; Scozzafava, A. *Curr. Med. Chem. Cardiovasc. Hematol. Agents* **2004**, *2*, 49−68.
(5) Tashian, R. E.; Venta, P. J.; Nicewander, P. H.; Hewett-Emmett, D. *Prog. Clin. Biol. Res.* **1990**, *344*, 159−175.
(6) Fujikawa-Adachi, K.; Nishimori, I.; Taguchi, T.; Onishi, S. *J. Biol. Chem.* **1999**, *274*, 21228−21233.
(7) Nishimori, I.; Onishi, S. *Dig. Liver Dis.* **2001**, *33*, 68−74.
(8) Marquis, R. E.; Whitson, J. T. *Drugs Aging* **2005**, *22*, 1−21.
(9) Vullo, D.; Innocenti, A.; Nishimori, I.; Pastorek, J.; Scozzafava, A.; Pastorekova, S.; Supuran, C. T. *Bioorg. Med. Chem. Lett.* **2005**, *15*, 963−969.
(10) Santos, M. A.; Marques, S.; Gil, M.; Tegoni, M.; Scozzafava, A.; Supuran, C. T. *J. Enzyme Inhib. Med. Chem.* **2003**, *18*, 233−242.
(11) Loiselle, F. B.; Morgan, P. E.; Alvarez, B. V.; Casey, J. R. *Am. J. Physiol. Cell Physiol.* **2004**, *286*, C1423−1433.
(12) Rivera, C.; Voipio, J.; Kaila, K. *J. Physiol.* **2005**, *562*, 27−36.
(13) Vullo, D.; Voipio, J.; Innocenti, A.; Rivera, C.; Ranki, H.; Scozzafava, A.; Kaila, K.; Supuran, C. T. *Bioorg. Med. Chem. Lett.* **2005**, *15*, 971−976.
(14) Lyons, K. E.; Pahwa, R.; Comella, C. L.; Eisa, M. S.; Elble, R. J.; Fahn, S.; Jankovic, J.; Juncos, J. L.; Koller, W. C.; Ondo, W. G.; Sethi, K. D.; Stern, M. B.; Tanner, C. M.; Tintner, R.; Watts, R. L. *Drug Saf.* **2003**, *26*, 461−481.
(15) Garske, L. A.; Brown, M. G.; Morrison, S. C. *J. Appl. Physiol.* **2003**, *94*, 991−996.
(16) Hori, K.; Ishida, S.; Inoue, M.; Shinoda, K.; Kawashima, S.; Kitamura, S.; Oguchi, Y. *Retina* **2004**, *24*, 481−482.
(17) Winum, J. Y.; Scozzafava, A.; Montero, J. L.; Supuran, C. T. *Med. Res. Rev.* **2005**, *25*, 186−228.
(18) Supuran, C. T. *Expert Opinion on Therapeutic Patents* **2003**, *13*, 1545−1550.

are highly overexpressed in tumors. We have recently reported[19,20] a class of fluorescent potent CAIs which specifically target hypoxic tumors in which the isoform CA IX is overexpressed. One of the most promising compounds in that series, derivative **1** (4-sulfamoylphenylethylthioureido)fluorescein, was shown to bind only to hypoxic tumors overexpressing various CA isozymes (such as CA IX and XII among others), which make it an important candidate for imaging purposes of this type of cancer. This compound, which is a strong inhibitor of the most physiologically relevant isozymes (CA II, K_i of 45 nM and CA IX, K_i of 24 nM, by a stopped-flow, CO_2 hydration assay method),[19,20] is in advanced clinical studies for its use as a diagnostic tool for the imaging and/or treatment of hypoxic tumors, which are nonresponsive to classical chemo- and radiotherapy.

Here we report the high resolution, X-ray crystal structure of compound **1** in complex with the cytosolic isoform II, together with a molecular modeling study on the adduct of **1** with the tumor-associated isoform IX, the main biological target for this type of derivative.[19,20] This combined approach gives a reasonable explanation for the experimentally observed different affinities of the fluorescent antitumor sulfonamide **1** toward hCA II and hCA IX, providing useful insights for the design of more isozyme-selective CA IX inhibitors with potential use as diagnostic tools in hypoxic tumors.

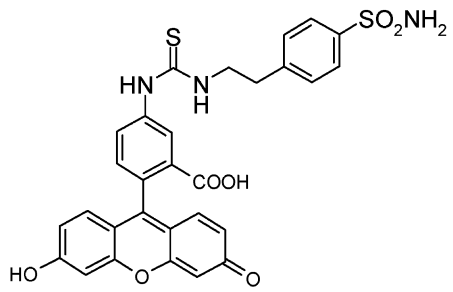

1

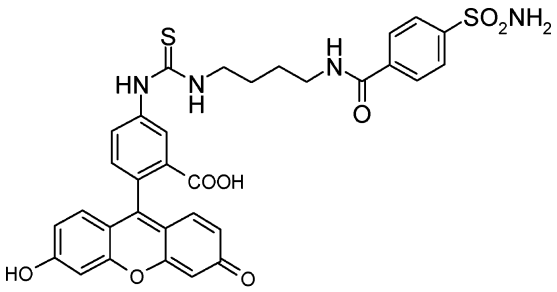

2

Results and Discussion

Chemistry and CA Inhibition. In addition to derivative **1** and its congeners prepared as fluorescent probes for hypoxic tumors,[19,20] CAIs incorporating fluorescein−thioureido moieties have already been reported earlier by Christianson's group[21] as probes for the fluorescence anisotropy detection of zinc ions, with a CA-based biosensor. Sulfonamide **2** has been reported in this pioneering study, being obtained by the coupling of fluorescein−isothiocyanate with 4-aminosulfonyl[1-(4-aminobutyl)]benzamide, i.e., by the same procedure subsequently used by our group for the preparation of the fluorescent probes for the imaging of hypoxic tumors.[20] The derivative described by Elbaum et al.[21] possesses a rather long spacer between the benzensulfonamide head which binds to CA and the fluorescein tail which confers the strong fluorescence. The corresponding spacer is on the other hand much shorter for our derivative **1**, just in order to investigate the binding possibility of the bulky fluorescein moiety within the enzyme active site cavity. Compound **2** was reported to behave as a very efficient hCA II inhibitor, with a dissociation constant K_d of 2.3 nM (determined by a fluorescence anisotropy binding assay).[21] To better compare our derivative (**1**) with the previously reported probe for the detection of zinc (compound **2**), we also measured the K_d of derivative **1** by the same procedure, using the fluorescence anisotropy assay.[21] In these conditions derivative **1** showed a K_d of 0.64 nM against hCA II and of 0.30 nM against hCA IX, being thus more effective than **2** as a hCA II inhibitor (**2** has not been tested as an hCA IX inhibitor). As it will be shown shortly, these results may be rationalized after considering the X-ray crystal structures of **1** and **2** in complex with hCA II.

Crystallographic Studies. Crystals of the hCA II−**1** adduct were isomorphous with those of the native protein,[22] allowing for the determination of the crystallographic structure by difference Fourier techniques. The model was refined using the CNS program[23] to crystallographic *R*-factor and *R*-free values of 0.168 and 0.197, respectively. The overall quality of the model was excellent, with 100% of the nonglycine residues located in the allowed regions of the Ramachandran plot. The statistics for data collection and refinement are summarized in Table 1.

Analysis of the three-dimensional structure of the complex revealed that the overall protein structure remained largely unchanged upon binding of the inhibitor. As a matter of fact, an rms deviation value of 0.29 Å was calculated over the entire Cα atoms of the hCA II−**1** complex with respect to the unbound enzyme. The analysis of the electron density maps around the catalytic site showed features compatible with the presence of one inhibitor molecule bound within the active site. The structure of the inhibitor **1** perfectly fit the shape of this electron density (Figure 1).

The main protein−inhibitor interactions are schematically depicted in Figure 1. It is observed that the tetrahedral geometry of the Zn^{2+} binding site and the key hydrogen bonds between the sulfonamide moiety of the inhibitor and enzyme active site were all retained with respect to other hCA II−sulfonamide complexes solved so far.[3,17] In particular, the ionized N atom of the sulfonamide group coordinated to zinc (1.95 Å), displacing the hydroxyl ion/water molecule present in the native enzyme.[22] This nitrogen atom was also involved in a hydrogen bond with the hydroxyl group of Thr199 (2.71 Å), which in turn interacted with the Glu106OE1 atom (2.52 Å). One sulfonamide oxygen (O1) accepted a hydrogen bond from the

(19) Svastova, E.; Hulikova, A.; Rafajova, M.; Zat'ovicova, M.; Gibadulinova, A.; Casini, A.; Cecchi, A.; Scozzafava, A.; Supuran, C. T.; Pastorek, J.; Pastorekova, S. *FEBS Lett.* **2004**, *577*, 439−445.
(20) Cecchi, A.; Hulikova, A.; Pastorek, J.; Pastorekova, S.; Scozzafava, A.; Winum, J. Y.; Montero, J. L.; Supuran, C. T. *J. Med. Chem.* **2005**, *48*, 4834−4841.
(21) Elbaum, D.; Nair, S. K.; Patchan, M. W.; Thompson, R. B.; Christianson, D. W. *Journal of the American Chemical Society* **1996**, *118*, 8381−8387.
(22) Eriksson, A. E.; Jones, T. A.; Liljas, A. *Proteins* **1988**, *4*, 274−282.
(23) Brunger, A. T.; Adams, P. D.; Clore, G. M.; DeLano, W. L.; Gros, P.; Grosse-Kunstleve, R. W.; Jiang, J. S.; Kuszewski, J.; Nilges, M.; Pannu, N. S.; Read, R. J.; Rice, L. M.; Simonson, T.; Warren, G. L. *Acta Crystallogr., Sect. D* **1998**, *54* (Pt 5), 905−921.

Table 1. Crystal Parameters, Data Collection, and Refinement Statistics for the HCA II−**1** Complex; Values in Parentheses Refer to the Highest Resolution Shell

Crystal Parameters	
space group	$P2_1$
unit-cell parameters (Å, deg)	$a = 42.26$
	$b = 41.60$
	$c = 72.22$
	$\beta = 104.57$
Data Collection Statistics (20.00−1.71 Å)	
temperature (K)	100
total reflections	67298
unique reflections	25716
completeness (%)	97.1 (93.4)
R-sym[a]	0.062 (0.235)
mean *I*/sigma(*I*)	12.9 (4.1)
Refinement Statistics (20.00−1.71 Å)	
R-factor[b] (%)	16.8
R-free[b] (%)	19.7
rmsd from ideal geometry:	
bond lengths (Å)	0.006
bond angles (deg)	1.37
number of protein atoms	2054
number of inhibitor atoms	41
number of water molecules	358
average *B* factor (Å^2)	16.5

[a] $R\text{-sym} = \Sigma|I_i - \langle I\rangle|/\Sigma I_i$; over all reflections. [b] $R\text{-factor} = \Sigma|F_o - F_c|/\Sigma F_o$; *R*-free calculated with 5% of data withheld from refinement.

backbone NH moiety of Thr199 (2.86 Å), while the other one (O2) was 3.02 Å away from the zinc ion, weakly contributing to its coordination site. The inhibitor organic scaffold did not establish polar interactions within the enzyme active site, as otherwise observed for some other hCA II−sulfonamide/sulfamate complexes,[24−27] but made a number of hydrophobic contacts. In particular, the phenethylthioureido moiety of **1** was oriented toward the hydrophobic part of the active site cleft (Figure 1), establishing strong van der Waals interactions (<4.5 Å) with residues Gln92, Val121, Phe131, Val135, Leu198, Thr199, Thr200, and Pro202. These residues were previously shown to be important for the binding of various benzenesulfonamide CAIs to hCA II.[26,28−31] On the other hand, the substituted 3-carboxy-amino-phenyl functionality of the inhibitor was at van der Waals distance from Phe131, Gly132, and Val135. The bulky tricyclic fluorescein moiety was located on the protein surface and strongly interacted with the α-helix formed by residues Asp130-Val135. Several van der Waals interactions with a symmetry-related enzyme molecule also contributed to the stabilization of the bulky fluorescein group in the investigated structure.

Figure 2 shows a structural overlay of **1** and the previously reported compound **2**[21] bound to hCA II, as determined by the superposition of hCA II active site residues. In both cases, the organic scaffold of the inhibitor did not establish direct polar interactions with the enzyme active site but participated in a large number of hydrophobic contacts. However, even though **1** and **2** are structurally similar, they showed important differences in their binding to the enzyme. In fact, while **1** was entirely defined in the electron density map as a result of the strong interaction with the enzyme, no electron density was observed for the fluorescein moiety present in compound **2**. A comparison of both complex structures suggested that the observed differences in the binding of these molecules to hCA II were related to the length of the molecular chain connecting the benzensulfonamide and fluoresceinyl moieties. In fact, **2** contained an additional butyleneaminocarbonyl group that limited the anchoring of the fluoresceinyl moiety to the enzyme active site, determining its protrusion toward the solvent and the absence of favorable interaction with amino acid residues present on the rim of the active site.

Modeling Studies. Models of hCA IX catalytic domain were obtained using both hCA II and mCA XIV[32] X-ray structures as templates either singly or in combination. As shown in the multiple alignment reported in Figure 3, hCA IX shows a higher sequence identity with mCA XIV (44% vs 34% for the alignment with hCA II), with only one gap of three residues at the C-terminus. Accordingly, the mCA XIV structure seemed a better template than the hCA II one, for modeling studies. However, also hCA II was utilized as a template as a consequence of the higher resolution of its X-ray structure and of the availability of the hCA II−**1** adduct crystal structure. All the hCA IX obtained models were subjected to 1 ns molecular dynamic simulations in solution and converged in a unique structural model. As already observed for other α-CAs for which the three-dimensional structure was solved,[33] this model consisted of a central ten-stranded β-sheet surrounded by several α-helices and additional β-strands (Figure 4). All geometrical arrangements of the residues coordinating the active site Zn^{2+} and hydrogen bond interactions between the zinc ligands (His94, His96 and His119, CA I numbering) and their protein environment were retained. As expected, the hCA IX three-dimensional model was very similar to that of hCA II (Figure 4). However, a detailed comparison between the two enzymes revealed a number of important local differences. Among these, the most important variation could be ascribed to the different orientation of the short helix region comprising amino acid residues 130−135 (Figure 4). The residue composition of this region was not conserved among the examined CAs (see Figure 3). In particular, a detailed analysis of the hCA II and hCA IX sequences highlighted a swapping in the position of basic and acidic residues (Asp130 → Arg and Lys133 → Glu).

On the basis of the high sequence/structural similarity between hCA IX and hCA II, it was not surprising that **1** showed rather small differences in the affinity toward both enzymes (as determined by two different assay procedures, a stopped-flow technique monitoring CO_2 hydration to bicarbonate,[20] and a fluorescence anisotropy method adapted from Elbaum et al.).[21] However for assessing the molecular basis of the differences

(24) Abbate, F.; Supuran, C. T.; Scozzafava, A.; Orioli, P.; Stubbs, M. T.; Klebe, G. *J. Med. Chem.* **2002**, *45*, 3583−3587.
(25) Abbate, F.; Casini, A.; Owa, T.; Scozzafava, A.; Supuran, C. T. *Bioorg. Med. Chem. Lett.* **2004**, *14*, 217−223.
(26) Abbate, F.; Winum, J. Y.; Potter, B. V.; Casini, A.; Montero, J. L.; Scozzafava, A.; Supuran, C. T. *Bioorg. Med. Chem. Lett.* **2004**, *14*, 231−234.
(27) Weber, A.; Casini, A.; Heine, A.; Kuhn, D.; Supuran, C. T.; Scozzafava, A.; Klebe, G. *J. Med. Chem.* **2004**, *47*, 550−557.
(28) Abbate, F.; Casini, A.; Scozzafava, A.; Supuran, C. T. *Bioorg. Med. Chem. Lett.* **2004**, *14*, 2357−2361.
(29) Abbate, F.; Coetzee, A.; Casini, A.; Ciattini, S.; Scozzafava, A.; Supuran, C. T. *Bioorg. Med. Chem. Lett.* **2004**, *14*, 337−341.
(30) Di Fiore, A.; De Simone, G.; Menchise, V.; Pedone, C.; Casini, A.; Scozzafava, A.; Supuran, C. T. *Bioorg. Med. Chem. Lett.* **2005**, *15*, 1937−1942.
(31) Menchise, V.; De Simone, G.; Alterio, V.; Di Fiore, A.; Pedone, C.; Scozzafava, A.; Supuran, C. T. *J. Med. Chem.* **2005**, *48*, 5721−5727.
(32) Whittington, D. A.; Grubb, J. H.; Waheed, A.; Shah, G. N.; Sly, W. S.; Christianson, D. W. *J. Biol. Chem.* **2004**, *279*, 7223−7228.
(33) Stams, T.; Christianson, D. W. *EXS* **2000**, 159−174.

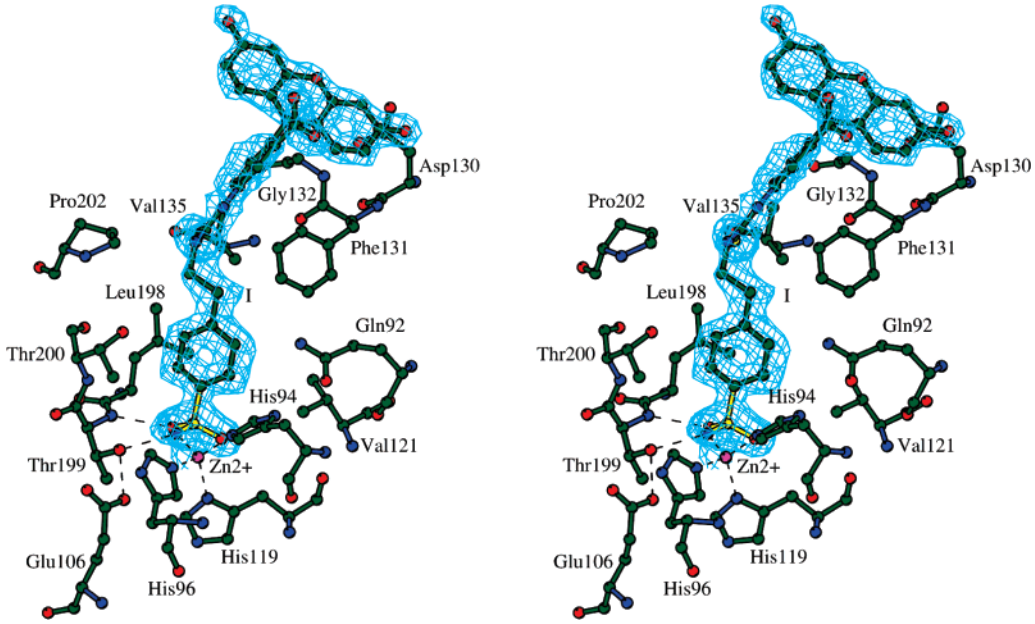

Figure 1. Stereoview of the active site region in the hCA II−**1** complex. The inhibitor (labeled I) is shown associated with simulated annealing omit $|2F_o - F_c|$ electron density map,[23] computed at 1.71 Å and contoured at 1.0 σ.

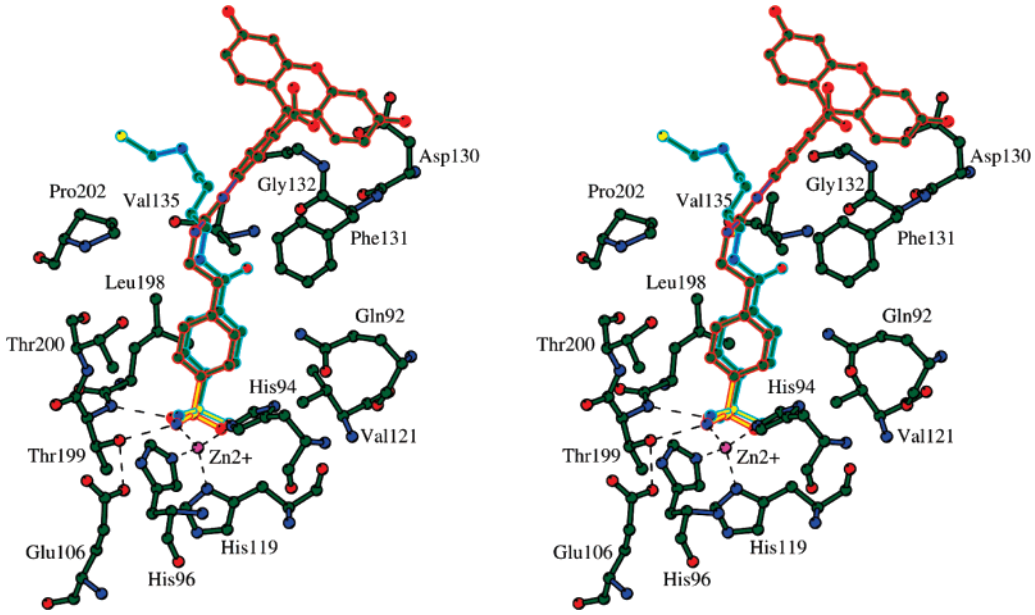

Figure 2. Stereoview of the hCA II active site complexed with **1** (contoured in red) and **2** (contoured in cyan) brought to optimal structural overlay. The fluorescein portion of inhibitor **2** is not reported since this part of the molecule was not defined in the electron density maps.

observed in K_I's (or K_d's) against the two CA isoforms, a model of the hCA IX−**1** complex was built up by homology modeling and molecular dynamics simulation approaches and compared to the structure of the corresponding complex with hCA II. The main protein−inhibitor interactions observed in the hCA IX complex are reported in Figure 5. Analysis of this figure reveals a conserved orientation of the active site residues involved in the binding of inhibitors/substrates, with all conserved H-bonds ensuring a proper catalytic machinery efficiency. Several polar and hydrophobic interactions stabilize the inhibitor within the hCA IX active site. In particular, the sulfonamide group of the inhibitor was bound to the enzyme active site in a manner similar to that observed in the hCA II−**1** complex. The phenylethylthioureido moiety established strong van der Waals interactions (<4.5 Å) with residues Gln92, Val121, Leu135, Leu198, Thr199, Thr200, and Pro202, while the substituted carboxyphenyl moiety of **1** was at van der Waals distance from Val131 and Asp132. All these contacts also strictly occurred in the hCA II−**1** complex structure. On the contrary, a unique polar interaction distinguished the hCA IX−**1** complex from the hCA II−**1** counterpart. In fact, also in this case the bulky tricyclic fluorescein functionality was located on the protein surface and strongly interacted with the α-helix formed by residues Arg130-Leu135. However the already described different orientation of this region and the mutation Asp130Arg caused the additional formation of a hydrogen bond between the arginine residue and the fluoresceinyl moiety of compound **1** (see Figure 5). Indeed, one of the guanidinium nitrogens of Arg130 hydrogen

```
hCA IX   12  GDPPWPRVSPACAGRFQSPVDIRPQLAAFCPALRPLELLGFQLPPLPELRLRNNGHSVQ
hCA XIV  12  GQDHWPTSYPECGGDAQSPINIQTDSVIFDPDLPAVQPHGYDQLGTEPLDLHNNGHTVQ
hCA II   12  GPEHWHKDFPIAKGERQSPVDIDTHTAKYDPSLKPLSVS-YDQA--TSLRILNNGHAFN

hCA IX   68  LTLPP---GLEMALG-PGREYRALQLHLHWGAAGRP-GSEHTVEGHRFPAEIHVVHLST
hCA XIV  68  LSLPP---TLHLGG--LPRKYTAAQLHLHWGQRGSLEGSEHHINSEATAAELHVVHYDS
hCA II   68  VEFDDSQDKAVLKGGPLDGTYRLIQFHFHWGSLDGQ-GSEHTVDKKKYAAELHLVHWNT

hCA IX  127  -AFARVDEALGRPGGLAVLAAFLEEGPEENSAYEQLLSRLEEIAEEGSETQVPGLDISA
hCA XIV 126  QSYSSLSEAAQKPQGLAVLGILIEVGETENPAYDHILSRLHEIRYKDQKTSVPPFSVRE
hCA II  127  -KYGDFGKAVQQPDGLAVLGIFLKVG-SAKPGLQKVVDVLDSIKTKGKSADFTNFDPRG

hCA IX  184  LLPSDFSRYFQYEGSLTTPPCAQGVIWTVFNQTVMLSAKQLHTLSDTLWGPGDSR---L
hCA XIV 184  LFPQQLEQFFRYNGSLTTPPCYQSVLWTVFNRRAQISMGQLEKLQETLSSTEEDPSEPL
hCA II  184  LLPESLD-YWTYPGSLTTPPLLECVTWIVLKEPISVSSEQVLKFRKLNFNGEGEPEELM

hCA IX  242  QLNFRATQPLNGRVIEASF
hCA XIV 242  VQNYRVPQPLNQRTIFASF
hCA II  242  VDNWRPAQPLKNRQIKASF
```

Figure 3. Sequence alignment used for modeling hCA IX, showing the sequence of hCA IX catalytic domain in comparison to those of hCA II and hCA XIV. Residues highly conserved in the three sequences are highlighted in red.

Figure 4. Superposition of the hCA IX homology model (gold) and the hCA II structure (violet). Residues belonging to the short helix region 130−135 and the Zn^{2+} ion coordination are represented as ball and stick.

bonds the carbonyl oxygen of the tricyclic ring belonging to the fluorescein moiety of the inhibitor. It is interesting to observe that independently from the Arg130 side chain starting orientation, all the 1 ns MD simulations carried out converged in a complex, which presented this stable hydrogen bond between Arg130 and the carbonyl group of compound **1**. This polar interaction which is absent in hCA II can be considered as the unique structural feature accounting for the observed differences in binding affinity of ligand **1** toward hCA II and hCA IX, but it is presumably quite important, since **1** is roughly 2 times a more effective inhibitor of the tumor-associated isozyme (hCA IX) over the cytosolic one (hCA II) and may account for the specific binding of **1** in vivo only to hypoxic tumors overexpressing CA IX and not to other tumor/normal tissue where other CA isozymes (such as CA II) may be present.[19]

Conclusion

We report here the high resolution X-ray crystal structure of the fluorescent antitumor sulfonamide CAI **1** in complex with the cytosolic isoform II, together with a modeling study on the adduct of **1** with the tumor-associated isoform hCA IX. The comparison of the two complex structures provides a reasonable explanation for the experimentally observed different affinities of **1** toward hCA II and hCA IX. Particularly, these results suggest that a different hydrogen bond network arrangement of hCA IX compared to hCA II accounts for the higher affinity of the inhibitor for the tumor-associated (CA IX) over the cytosolic (CA II) isozyme. The guanidine moiety of Arg130, which is an amino acid specific to CA IX, participates in a hydrogen bond with the carbonyl oxygen of the fluorescein tail of the inhibitor. The observed different binding modes of this fluorescent sulfonamide to CA IX and CA II allow for the further drug design of more isozyme-selective CA IX inhibitors with potential use as diagnostic tools or for the management of hypoxic tumors.

Experimental Protocols

Chemistry and CA Inhibition. Compound **1** was prepared as described earlier,[20] by reaction of fluorescein isothiocyanate (Sigma-Aldrich, Milan, Italy) and 4-aminoethylbenzenesulfonamide (Sigma-Aldrich, Milan, Italy). The inhibition constants for the physiological reaction catalyzed by the enzyme, i.e., CO_2 hydration to bicarbonate and a proton, were reported earlier, both against hCA II and IX.[20] In addition, the dissociation constant (K_d) of **1** against hCA II or hCA IX has been determined by the fluorescence anisotropy assay, as reported by Christianson's group.[21] A solution of **1** (30 nM) was prepared in 100 mM Tris-sulfate buffer (pH 8.0, 24 °C) and was used as a stock solution of inhibitor. Recombinant hCA II/hCA IX were serially diluted with the stock solution of **1**, working at enzyme concentrations in the range 5−300 nM, and were analyzed by the fluorescence anisotropy in triplicate experiments, with a Perkin-Elmer lambda 50B spectrofluorometer. Using the eqs 1−5 derived by Christianson's group for the fitting of the measured anisotropy as a function of the total concentration of enzyme ($[E]_t$) and inhibitor ($[I]_t$),

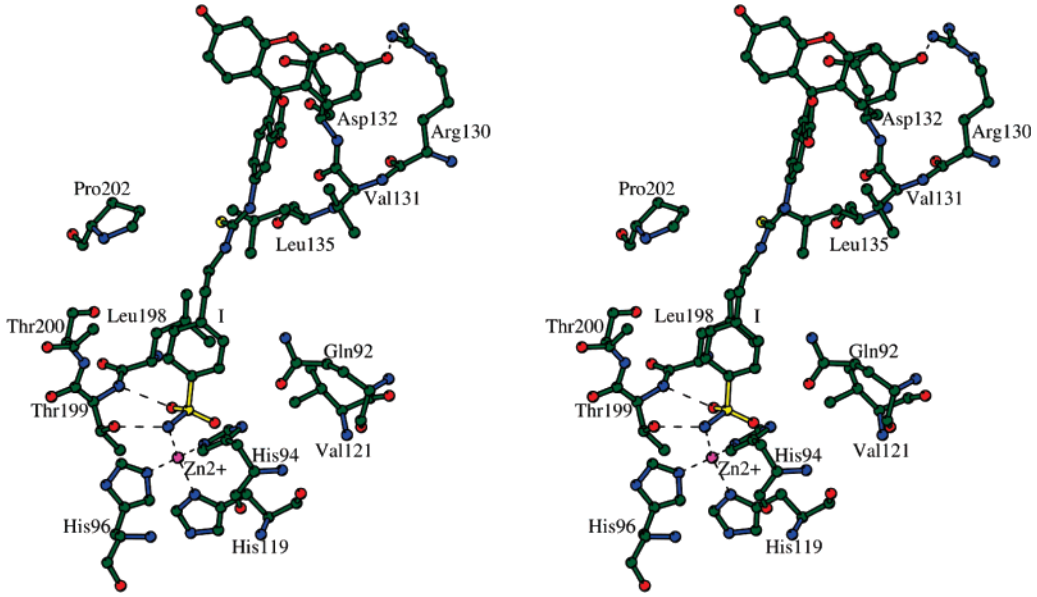

Figure 5. Stereoview of the active site region in the hCA IX−**1** complex showing the residues participating in the recognition of the inhibitor molecule. Hydrogen bonds and the active site Zn^{2+} ion coordination are also shown (dotted lines).

the K_d of the inhibitor is obtained[21] as follows:

$$K_d = [E][I]/[E-I] \quad (1)$$

where [E] = enzyme concentration at equilibrium, [I] = inhibitor concentration at equilibrium, and [E−I] = concentration of the enzyme−inhibitor adduct at equilibrium. Considering that

$$[E]_t = [E] + [E-I] \quad (2)$$

$$[I]_t = [I] + [E-I] \quad (3)$$

$$r_0 = f_b r_b + f_f r_f \quad (4)$$

(where r_0 is the observed fluorescence anisotropy, r_f, the anisotropy of inhibitor when free, and r_b, anisotropy of inhibitor when bound to the enzyme), by rearranging eqs 1−4, one obtains

$$r_0 - r_f = (r_b - r_f)\{[([I]_t + [E]_t + K_d) - \{([I]_t + [E]_t + K_d)^2 - 4[I]_t[E]_t\}^{1/2}]/2[I]_t\} \quad (5)$$

where f_b, f_f = fraction of bound and free fluorophore, respectively; r_b, r_f = the anisotropy of the bound and free fluorophore, respectively, where the unitless quantity r, anisotropy, is defined as[21]

$$r = (I_{II} - I_\perp)/(I_{II} + 2I_\perp)$$

(I_{II} and $I_\perp$ are the intensity of the emission parallel and perpendicular to the excitation polarization, respectively).

Thus, fitting the anisotropies measured as a function of the total concentration of enzyme to eq 5 yields the K_d of the inhibitor. The curve fitting has been performed with the program PRISM 4.

Crystallization, X-ray Data Collection, and Refinement. Crystals of the hCA II−**1** complex were obtained by soaking enzyme crystals[22] (monoclinic crystal form, space group $P2_1$) in a solution containing 20 mM inhibitor in the crystallization buffer. A complete dataset was collected at 1.71 Å resolution from a single crystal, at 100 K, at Synchrotron source Elettra in Trieste, using a Mar CCD detector. Prior to cryogenic freezing crystals were transferred to the precipitant solution with the addition of 15% (v/v) glycerol. Diffracted intensities were processed using the HKL crystallographic data reduction package (Denzo/Scalepack).[34] A total of 67 298 reflections were measured and reduced to 25 716 unique reflections. Crystal parameters and data processing statistics are summarized in Table 1. The structure of the complex was analyzed by difference Fourier techniques using hCA II crystallized in the $P2_1$ space group (PDB code 1CA2[22]) as the starting model. Water molecules were removed from the starting model prior to structure factor and phase calculations. The crystallographic *R*-factor and *R*-free, calculated in the 20.00−1.71 Å resolution range, based on the starting model coordinates, were 0.350 and 0.381, respectively. Fourier maps calculated with $3F_o - 2F_c$ and $F_o - F_c$ coefficients (F_o are the observed structure factors for the complex, and F_c, those calculated on the basis of the model atomic coordinates) showed prominent electron density features in the active site region. After an initial refinement, limited to the enzyme structure (*R*-factor 0.193 and *R*-free 0.236), a model for the inhibitor was easily built and introduced into the atomic coordinates set for further refinement, which proceeded to convergence with continuous map inspection and model updates. The refinement was carried out with the program CNS;[23] model building and map inspections were performed using the O program.[35] Final crystallographic *R*-factor and *R*-free values calculated for the 25 127 observed reflection were 0.168 and 0.197, respectively. The correctness of stereochemistry was finally checked using PROCHECK.[36] Statistics for refinement are summarized in Table 1. Coordinates and structure factors have been deposited with the Protein Data Bank (accession code 2F14).

Modeling Studies and Molecular Dynamics Simulations. The hCA IX sequence was retrieved from the publicly available sequence database Swiss-Prot/TrEMBL[37] (primary accession number Q16790). On the basis of a sequence search against the PDB by using PSI-BLAST,[38] the X-ray structures of mCA XIV (PDB entry 1RJ6)[32] and hCA II were identified as the best structural templates to model the corresponding catalytic domain (Gly12-Phe260) of hCA IX either singly or in combination. Pairwise and multiple alignments between templates and

(34) Otwinowski, Z.; Minor, W. *Methods in Enzymology* **1997**, *276*, 307−326.
(35) Jones, T. A.; Zou, J. Y.; Cowan, S. W.; Kjeldgaard *Acta Crystallogr., Sect. A* **1991**, *47* (Pt 2), 110−119.
(36) Laskowski, R. A.; MacArthur, M. W.; Moss, D. S.; Thornton, J. M. *Journal of Applied Crystallography* **1993**, *26*, 283−291.
(37) Boeckmann, B.; Bairoch, A.; Apweiler, R.; Blatter, M. C.; Estreicher, A.; Gasteiger, E.; Martin, M. J.; Michoud, K.; O'Donovan, C.; Phan, I.; Pilbout, S.; Schneider, M. *Nucleic Acids Res.* **2003**, *31*, 365−370.
(38) Altschul, S. F.; Madden, T. L.; Schaffer, A. A.; Zhang, J.; Zhang, Z.; Miller, W.; Lipman, D. J. *Nucleic Acids Res.* **1997**, *25*, 3389−3402.

the target sequence were carried out with CLUSTALW.[39] For each pairwise and multiple alignment 50 homology models were built with MODELLER[40] and their qualities were assessed using PROCHECK[36] and the 3D-profile[41] module of INSIGHT II (Accelrys Software Inc.). The best models obtained using hCA II and mCA XIV as templates singly showed the same *G*-factor value of PROCHECK (−0.14) and a similar 3D-profile index. A better model was obtained using both templates simultaneously. This model showed a positive *G*-factor value (0.54) and a good 3D-profile index (112.23 to be compared with an expected value for a protein of this length of 111.76 and a threshold value of 50.29, below which the model is wrong). All selected models were complexed with ligand **1**, whose starting coordinates were derived from the hCA II−**1** X-ray structure. Complexes were completed by addition of all hydrogen atoms and were subjected to energy minimization with the SANDER module of the AMBER8 package[42] using the PARM99 force field.[43]

Atomic charges of molecule **1** were obtained with RESP methodology.[44] The conformation of ligand **1** derived from the hCA II−**1** crystal structure was fully optimized using the GAMESS program[45] at the Hartree−Fock level with the STO-3G basis set. Single-point calculations on the optimized molecule were performed at the RHF/6-31G* level. The resulting electrostatic potential was thus used for a two-stage single-conformation RESP charge fitting. Partial charges for the three catalytic histidines and Zn^{2+} were those published by Suarez and Merz.[46] To preserve the integral charge of the whole system, partial charges of Cα and Hα atoms of the Zn^{2+}−ligand residues and of N and H atoms of the inhibitor sulfonamide group were modified accordingly. A bonded approach between the Zn^{2+} ion and its ligands was adopted to preserve the experimentally observed tetrahedral Zn^{2+} coordination in all complexes during MD simulations. Equilibrium bond distances and bond angles involving the Zn^{2+} ion were derived from the hCA II−**1** crystal structure. Force constants of 120 kcal mol^{-1} Å^{-1} were used for N(His)−Zn^{2+} bond parameters, while force constants of 20 and 30 kcal mol^{-1} Å^{-1} were adopted for N(His)−Zn^{2+}−N(His) and N(His)−Zn−N(sulfonamide) angle parameters, respectively. All the torsional parameters associated with interactions between Zn^{2+} and its ligands were set to zero as in the case for Hoops et al.[47]

To perform MD simulations in solvent, minimized models were confined in truncated octahedral boxes filled with TIP3P water molecules and counterions (Na^+) to ensure electrostatic neutrality. The solvated molecules were then energy minimized through 1000 steps with solute atoms restrained to their starting positions, using a force constant of 10 kcal mol^{-1} Å^{-1} prior to MD simulations. The molecules were then submitted to 90 ps restrained MD (5 kcal mol^{-1} Å^{-1}) at constant volume, gradually heating to 300 K, followed by 60 ps restrained MD (5 kcal mol^{-1} Å^{-1}) at constant pressure to adjust system density. MD production runs were carried out at 300 K for 1 ns with a time step of 1.5 fs. Bonds involving hydrogens were constrained using the SHAKE algorithm.[48] Snapshots from production runs were saved every 1000 steps and analyzed with the MOLMOL program.[49]

Acknowledgment. This research was financed in part by a grant from the 6th framework of EU (EUROXY project). We would like to thank Sincrotrone Trieste CNR/Elettra, for giving us the opportunity to collect data at the Crystallographic Beamline.

JA061574S

(39) Thompson, J. D.; Higgins, D. G.; Gibson, T. J. *Nucleic Acids Res.* **1994**, *22*, 4673−4680.
(40) Sali, A.; Blundell, T. L. *J. Mol. Biol.* **1993**, *234*, 779−815.
(41) Bowie, J. U.; Luthy, R.; Eisenberg, D. *Science* **1991**, *253*, 164−170.
(42) Pearlman, D. A.; Case, D. A.; Caldwell, J. W.; Ross, W. S.; Cheatham, T. E., III; DeBolt, S.; Ferguson, D.; Seibel, G.; Kollman, P. *Computer Physics Communications* **1995**, *91*, 1−42.
(43) Wang, J.; Cieplak, P.; Kollman, P. A. *Journal of Computational Chemistry* **2000**, *21*, 1049−1074.
(44) Bayly, C. I.; Cieplak, P.; Cornell, W.; Kollman, P. A. *Journal of Physical Chemistry* **1993**, *97*, 10269−10280.
(45) Schmidt, M. W.; Baldridge, K. K.; Boatz, J. A.; Elbert, S. T.; Gordon, M. S.; Jensen, J. H.; Koseki, S.; Matsunaga, N.; Nguyen, K. A.; Su, S.; Windus, T. L.; Dupuis, M.; Montgomery J. A. *Journal of Computational Chemistry* **1993**, *14*, 1347−1363.
(46) Suarez, D.; Merz, K. M., Jr. *J. Am. Chem. Soc.* **2001**, *123*, 3759−3770.
(47) Hoops, S. C.; Anderson, K. W.; Merz, K. M., Jr. *Journal of the American Chemical Society* **1991**, *113*, 8262−8270.
(48) Ryckaert, J. P.; Ciccotti, G.; Berendsen, H. J. C. *Journal of Computational Physics* **1977**, *23*, 327−341.
(49) Koradi, R.; Billeter, M.; Wuethrich, K. *Journal of Molecular Graphics* **1996**, *14*, 51−55, plates, 29−32.